Simultaneous UV Images and High-latitude Particle and Field Measurements During an Auroral Dawn Storm at Jupiter

R. W. Ebert[1,2], T. K. Greathouse[1], G. Clark[3], V. Hue[1], F. Allegrini[1,2], F. Bagenal[4], S. J. Bolton[1], B. Bonfond[5], J. E. P. Connerney[6,7], G. R. Gladstone[1,2], M. Imai[8], S. Kotsiaros[10], W. S. Kurth[9], S. Levin[11], P. Louarn[12], B. H. Mauk[3], D. J. McComas[13], C. Paranicas[3], A. H. Sulaiman[9], J. R. Szalay[13], M. F. Thomsen[14], and R. J. Wilson[4]

[1]Southwest Research Institute, San Antonio, Texas, USA
[2]Department of Physics and Astronomy, University of Texas at San Antonio, San Antonio, Texas, USA
[3]Johns Hopkins University Applied Physics Lab, Laurel, Maryland, USA
[4]Laboratory for Atmospheric and Space Physics, University of Colorado Boulder, Boulder, Colorado, USA
[5]Université de Liège, Liège, Belgium
[6]Space Research Corporation, Annapolis, MD
[7]NASA Goddard Space Flight Center, Greenbelt, MD
[8]Department of Electrical Engineering and Information Science, National Institute of Technology, Niihama College, Niihama, Ehime, Japan
[9]Department of Physics and Astronomy, University of Iowa, Iowa City, IA, USA
[10]DTU Space, Technical University of Denmark, Kgs. Lyngby, Denmark
[11]Jet Propulsion Laboratory, Pasadena, California, USA
[12]Institut de Recherche en Astrophysique et Planétologie, Toulouse, France
[13]Department of Astrophysical Sciences, Princeton University, Princeton, New Jersey, USA
[14]Planetary Science Institute, Tucson, Arizona, USA

Key Points

1. Juno concurrently observed UV emissions from a Jupiter dawn storm and high-latitude plasma mapping to them at radial distances of ~6 – 8 R_J.

2. Electron distributions with energies from ~10–1000 keV carried a significant fraction of the energy flux needed to produce the UV emissions.

3. Energetic ions, magnetic perturbations, whistler mode waves and bKOM radio emissions were observed on field lines mapping to the dawn storm.

Abstract

We present multi-instrument Juno observations on day-of-year 86, 2017 that link particles and fields in Jupiter's polar magnetosphere to transient UV emissions in Jupiter's northern auroral region known as *dawn storms*. Juno ranged from 42ºN - 51ºN in magnetic latitude and 5.8 – 7.8 jovian radii (1 R_J = 71,492 km) during this period. These dawn storm emissions consisted of two separate, elongated structures which extended into the nightside, rotated with the planet, had enhanced brightness (up to at least 1.4 megaRayleigh) and high

color ratios. The color ratio is a proxy for the atmospheric penetration depth and therefore the energy of the electrons that produce the UV emissions. Juno observed electrons and ions on magnetic field lines mapping to these emissions. The electrons were primarily field-aligned, bi-directional, and, at times, exhibited sudden intensity decreases below ~10 keV coincident with intensity enhancements up to energies of ~1000 keV, consistent with the high color ratio observations. The more energetic electron distributions had characteristic energies of ~160 – 280 keV and downward energy fluxes (~70 – 135 mW/m^2) that were a significant fraction needed to produce the UV emissions for this event. Magnetic field perturbations up to ~0.7% of the local magnetic field showing evidence of upward and downward field-aligned currents, whistler mode waves, and broadband kilometric radio emissions were also observed along Juno's trajectory during this timeframe. These high latitude observations show similarities to those in the equatorial magnetosphere associated with dynamics processes such as interchange events, plasma injections, and/or tail reconnection.

1. Introduction

The primary components of Jupiter's ultraviolet (UV) aurora are the main, outer, polar, and satellite emissions [see review by Grodent et al., 2015 for details]. These emissions are produced primarily by precipitating electrons interacting with H_2 molecules in Jupiter's upper atmosphere [e.g. Broadfoot et al., 1979] and can be used as a diagnostic of dynamics and structure in Jupiter's magnetosphere. A number of secondary, transient UV auroral emissions have also been identified, many occurring in the dawn sector of Jupiter's auroral region [e.g. Prangé et al., 1993; Gérard et al., 1994; Ballester et al., 1996; Clarke et al., 1998; Gustin et al. 2006; Radioti et al., 2008; Kimura et al., 2015; 2017; Yao et al. 2020; Bonfond et al., 2021].

Using UV images from the Faint Object Camera on the Hubble Space Telescope (HST), Gérard et al., [1994] identified a bright, arc-like UV feature of ~6 megarayleighs (MR) in Jupiter's northern auroral region that was in quasi-corotation with the planet. This feature dimmed by more than an order of magnitude when it was observed again ~20 hours later, suggesting a transient phenomenon that was attributed to large-scale variations in Jupiter's magnetospheric current system. Clarke et al., [1998] identified bright, transient UV emissions in the local dawn region near the expected location of Jupiter's main emission. These emissions, coined 'dawn storms', showed significant spreading in longitude and remained near local dawn while other, dimmer, emissions co-rotated with the planet. Their proximity to the main aurora suggested that these emissions were produced in Jupiter's middle magnetosphere. Kimura et al., [2015] interpreted these dawn storms as being driven by tail reconnection, bringing energetic particles from the outer and middle magnetosphere to the inner magnetosphere within a timeframe of up to 2 planetary rotations. Gustin et al., [2006] reported on dawn UV auroral brightenings of up to ~1.8 MR, approximately 4 times brighter than the nominal main emission [Grodent et al., 2003]. These features had a leading edge that was fixed in system III longitude (a system fixed with the corotationg planet) whereas the trailing edge seemed to be organized by local time, with an extension into the nightside of Jupiter's auroral region. UV spectral observations were used to infer the characteristic energies (up to ~50 – 500 keV), energy fluxes (5 – 90 mW m^{-2}) and

current densities (~0.1 – 0.5 μA m^{-2}) of the precipitating electrons responsible for producing these emissions [Gustin et al., 2006]. These electrons were interpreted as being accelerated by electric fields in regions of upward field-aligned currents.

In July 2016, NASA's Juno mission [Bolton et al., 2017] was inserted into a 53-day polar orbit around Jupiter. Juno is a spinning spacecraft with a ~30 s spin period. Its orbit and suite of instruments provide an excellent platform to remotely image Jupiter's aurora [e.g. Connerney et al., 2017a] while simultaneously measuring in situ the polar magnetospheric environment that map to unique auroral emissions [e.g. Ebert et al., 2019; Gérard et al., 2019]. The Juno observations present a new opportunity to study the physics of dawn storms at Jupiter. For instance, Bonfond et al. [2021] examined the complete process of dawn storm evolution using global images of these events provided by Juno along with their frequency. They found that dawn storms originate as small, short-lived emissions followed a couple of hours later by the evolution from a linear to a more irregular arc in the main emission in the midnight region which then rotates toward dawn. After broadening and then splitting, these emissions are separated by a region absent of emissions that fills in as the event progresses. The final stage produces equatorward-moving auroral emissions associated with plasma injection signatures. Considered as a sequence, these auroral features were interpreted as the signature of magnetotail reconfigurations, including reconnection, plasma instabilities, dipolarization, and plasma injections. They also determined that dawn storms are present in approximately half of the 8-hour long perijove sequences during Juno's first 20 perijoves.

Yao et al. [2020] combined in situ particle and field measurements in Jupiter's equatorial magnetosphere from Juno with auroral observations from the HST. They found that auroral dawn storm emissions were often observed in conjunction with auroral signatures attributed to particle injections in the equatorial magnetosphere. They suggested that the drivers of these emissions may be physically connected, with magnetic reconnection in the dawn side magnetosphere being responsible for the auroral dawn storms and the subsequent magnetic dipolarization producing the auroral injection signatures. Swithenbank-Harris et al. [2021] also examined in-situ measurements from Juno in Jupiter's equatorial dawn magnetosphere concurrent with an auroral dawn storm observed by HST. Their analysis revealed a source region located at ~60 R_J with a component rotating towards local noon and proton velocities to near corotation speeds. The source region was characterized by enhanced densities of hot plasma, field-aligned energetic protons and heavy ions, and a reversal in the azimuthal component of Jupiter's magnetic field. They suggested that dawn storms result from the acceleration and heating of magnetospheric plasma following reconnection at earlier local times.

In this study, we present UV images and in situ particle and field observations in Jupiter's polar magnetosphere associated with a dawn storm in Jupiter's northern auroral region on day-of-year (DOY) 86, 2017, prior to Juno's 5th perijove (PJ5). We focus on the period from 03:00 – 05:00 UT when Juno ranged from 7.8 R_J to 5.8 R_J in jovicentric radial distance and 41.6°N to 50.9°N in magnetic latitude. This period is of high interest because the spacecraft simultaneously imaged the UV emissions it was magnetically connected to. This was the first time that Juno was at high latitude and on magnetic field lines connecting to

a dawn storm. Section 2 provides an overview of the Juno data sets and observing geometry used in this study. UV brightness and color ratio images and polar magnetosphere particle and field observations are presented in section 3. Section 4 provides an interpretation of the observations. A summary and conclusions are presented in Section 5. These Juno observations provide a unique opportunity to study particle and field features at high latitude that directly map to transient UV emissions observed in Jupiter's dawn auroral region.

2. Data Sets and Observing Geometry

We examine electron and ion observations from Juno's Jovian Auroral Distributions Experiment Electron (JADE-E) and Ion (JADE-I) sensors [McComas et al., 2017] and Jupiter Energetic particle Detector Instrument (JEDI) [Mauk et al. 2017a], UV emissions from Juno's Ultraviolet Spectrograph (UVS) [Gladstone et al., 2017], radio and plasma wave observations from the Waves instrument [Kurth et al. 2017], and magnetic field observations from the Magnetic Field Investigation (MAG) [Connerney et al. 2017b]. JADE-E and JEDI measure electron fluxes in the energy range of 0.1 – 100 keV and 30 – 1000 keV, respectively, along with their pitch angle distributions, with a time resolution up to 1 s. JADE-I measures ions from 0.01 – 46 keV/charge (keV/q) over a mass per charge (m/q) range of ~1 – 64 amu at a time resolution as high as 2 s. JEDI measures ions with total energy from ~50 keV to well above 1 MeV (upper limit is species dependent), along with their pitch angle distributions and can resolve oxygen and sulfur above ~400 keV. UVS is an imaging spectrograph sensitive to wavelengths between 68 and 210 nm. It observes Jupiter's northern and southern auroras for several hours bounding each Juno perijove pass from jovicentric distances of ~1.3 – 7 R_J. A scan mirror allows shifting the field-of-view (FOV) of UVS by up to ±30° above or below the spacecraft spin plane. The combination of Juno's spinning nature and UVS's scan mirror gives this instrument access to half the sky for any given spacecraft orientation. The UV brightness is determined by integrating the emissions between 155 – 162 nm and then multiplying by 8.1 to estimate the total H_2 emission between 75 – 198 nm [Gérard et al., 2019]. Waves measures the wave magnetic and electric fields covering frequency ranges of 50 Hz – 20 kHz and 50 Hz – 40 MHz, respectively, at a time resolution of up to 1 s near Juno's perijove. MAG consists of two independent sensor suites, each containing a tri-axial fluxgate magnetometer (FGM) and a pair of imaging sensors. The FGMs simultaneously measure the magnetic field at a rate of 64 vector samples per second. We utilize 1 s magnetic field vector observations from MAG to calculate the electron pitch angle distributions. See the instrument papers cited above for more details.

Figure 1 shows Juno's trajectory on approach to PJ5 and its projection onto the planet using the JRM09 internal magnetic field model [Connerney et al., 2018] and the magnetodisc model of Connerney et al., [1981], where Z_{MAG} is along Jupiter's magnetic dipole axis and ρ_{MAG} is the perpendicular distance from the magnetic dipole axis. M, or M-shell, corresponds to a distance based on the predicted magnetic equator crossing distance for any given magnetic field line. Juno's magnetic footpoint maps along Jupiter's northern main auroral oval from ~02:00 – 06:30 UT on DOY 086, 2017. The periods of interest are highlighted by the thick red, blue, and green lines. The blue line corresponds to an interval

when Juno made in situ measurements of particles, and fields while simultaneously observing bright UV features near Jupiter's main emission. The red line identifies a period when Juno made in-situ measurements on field lines mapping to the expected location of the bright UV features under consideration here. The green line highlights when Juno was only remotely observing the bright UV auroral features.

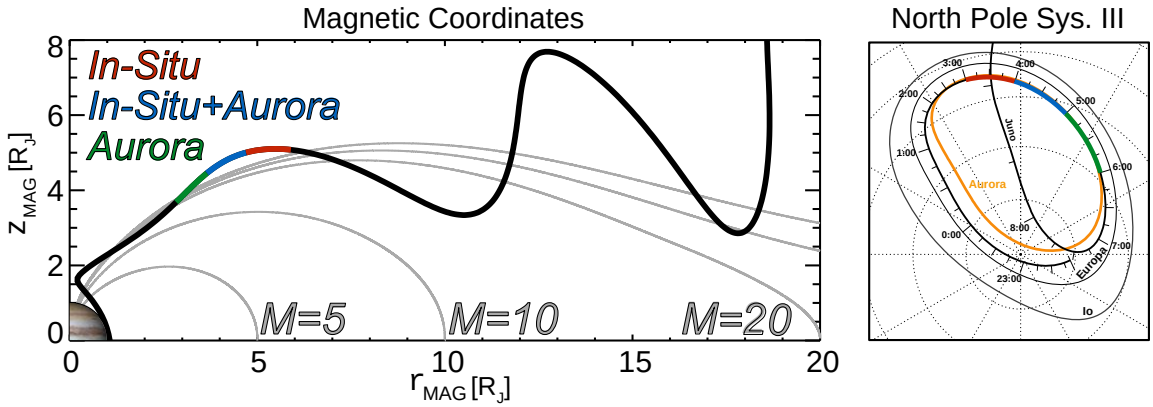

Figure 1: *(Left) Juno's inbound trajectory (black line) in Jupiter's northern hemisphere prior to perijove 5 on days-of-year 85 – 86, 2017. The trajectory is shown in a magnetic coordinate system [Connerney et al., 1981; 2018]. Magnetic field lines, and the M-shells that they map to, are shown in grey. (Right) Magnetic projection of Juno's trajectory onto the 1-bar level of Jupiter's upper atmosphere in black with times indicated. Orange oval denotes the statistical average position of Jupiter's main ultraviolet aurora [Bonfond et al., 2012]. Thick red, blue, and green lines highlight the periods of interest along Juno's trajectory. Dashed circles and lines are contours of constant jovicentric latitude and system III longitude, respectively. Black ovals identify the location of the Io (outer) and Europa (inner) auroral footprint paths.*

3. UV Aurora and High-Latitude Magnetosphere Observations

Figure 2 presents UV brightness (left column) and color ratio (right column) maps of Jupiter's northern auroral region covering the period from 03:58 – 06:06 UT on DOY 86, 2017. Each map is a composite of 12 different images obtained over a ~6-minute interval, each image having ~17 ms of integration time. The color ratio, defined as the ratio between the integrated brightness from 158 to 162 nm and 126 to 130 nm, is used to estimate the depth from which the UV emissions are generated and are a proxy for the characteristic energy of the precipitating electrons that produce them. A larger color ratio is interpreted as representing more energetic electrons that produce the UV emissions [e.g. Gérard and Singh, 1982], with more energetic electrons penetrating deeper into the atmosphere [e.g. Gérard et al., 2014].

This study focuses on the bright UV emissions observed on the left side of Figure 2(a), near the statistical average latitude of the main aurora, denoted by the white dashed ovals [Bonfond et al., 2012]. These UV emissions consist of two bright, elongated features on the dawn side of the auroral region, a leading spot near the terminator, and a trailing spot on the nightside. Figures 2(a) – 2(e) are a time series of the auroral images and show that

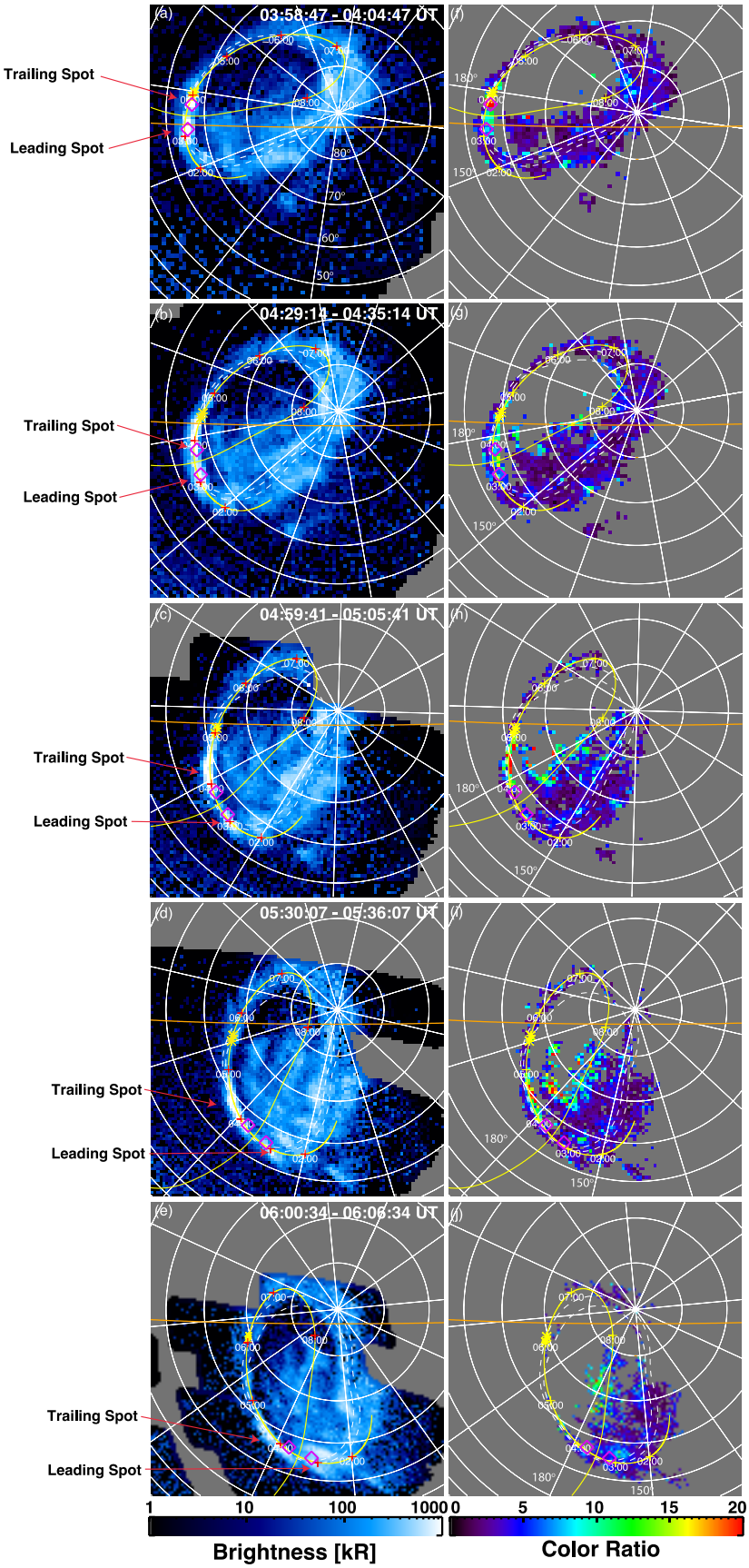
(a)
03:58:47 - 04:04:47 UT
(f)
Trailing Spot
Leading Spot
(b)
04:29:14 - 04:35:14 UT
(g)
Trailing Spot
Leading Spot
(c)
04:59:41 - 05:05:41 UT
(h)
Trailing Spot
Leading Spot
(d)
05:30:07 - 05:36:07 UT
(i)
Trailing Spot
Leading Spot
(e)
06:00:34 - 06:06:34 UT
(j)
Trailing Spot
Leading Spot
1
10
100
1000
Brightness [kR]
0
5
10
15
20
Color Ratio

221

Figure 2: *(a) – (e) Polar projections of ultraviolet (UV) brightness images in Jupiter's northern auroral region on day-of-year 086, 2017 from 03:58 to 06:06 UT. (f) – (j) Color ratio images for the same intervals as shown for the UV brightness. These images are in chronological order. Red arrows in (a) – (e) point to the emissions studied here. Yellow lines identify Juno's trajectory, the yellow stars identify Juno's footprint at the time when the UV images were collected. The purple diamonds in each panel bound the latitude and longitude for the UV emissions whose brightness and color ratio estimates are shown in Figure 3. Orange lines denote the day-night terminator, the Sun direction being the bottom of each image. The two white dashed lines represent the statistical average compressed and expanded position of Jupiter's main ultraviolet (UV) aurora [Bonfond et al., 2012].*

these features travel in the direction of planetary rotation. The purple diamond symbols in Figure 2 identify emissions that are tracked throughout this interval, at a System-III latitude and longitude of 55.6° and 165.3°, respectively, for the leading spot and 56.8° and 174.8°, respectively, for the trailing spot (see Figure 3).

The image in Figure 2(f) indicates that the UV features under consideration have relatively high color ratios compared to the surrounding emissions. The color ratio for the nightside emission is greater than that for the emission near the terminator, suggesting that the nightside emissions are produced by more energetic electrons. Figures 2(f) – 2(i) show that the color ratio for the trailing spot remains relatively higher than the leading spot throughout most of the interval.

Figure 3 shows a time series of the maximum brightness and color ratio for the UV emissions at the latitudes and longitudes specified within the purple diamond symbols in Figure 2, along with their uncertainties. We present a value from each image shown in Figure 2. The maximum brightness at the locations specified for the leading and trailing spots were 1170 ± 290 kilorayleighs (kR) and 1380 ± 300 kR, respectively, at the beginning of the interval and 660 ± 240 kR and 100 ± 100 kR, respectively, at the end of the interval. The maximum color ratio for the leading spot ranged between 5.7 – 8.5 within the region of interest. The maximum color ratio within the trailing spot at the beginning of the interval was significantly higher compared to the leading spot and remained relatively enhanced except for the last image. This indicates that electrons producing the trailing spot were more energetic than those producing the leading spot. The brightness and color ratio within both the leading and trailing spots showed a reduction in magnitude as the dawn storm progressed.

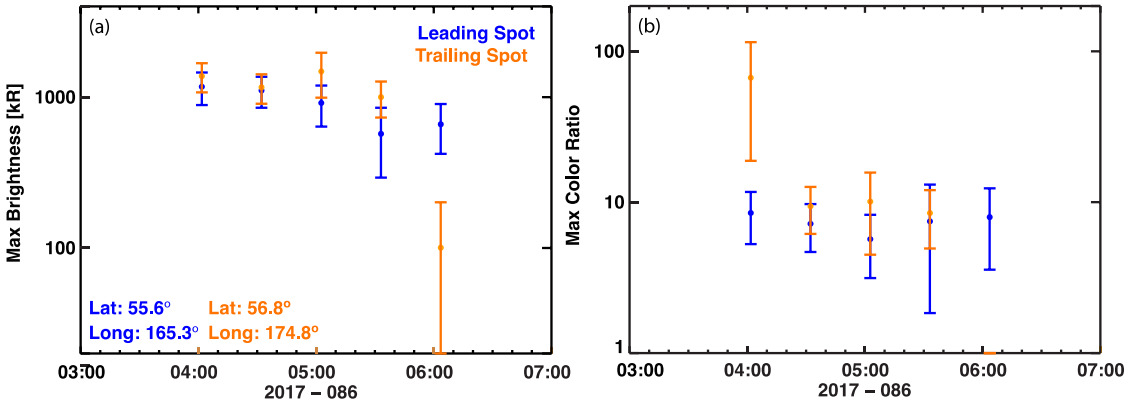

Figure 3: *(a) Maximum (max) UV brightness and (b) max color ratio within the latitudes and longitudes within the region bound by the purple diamond symbols in Figure 2..*

Figure 4 presents UV aurora and polar magnetosphere electron, ion, and magnetic field observations from DOY 086, 2017. The UV brightness (Figure 4a) and color ratio (Figure 4b) images were obtained from observations collected between 03:58 and 04:04 UT, a period when Juno's magnetic footprint mapped to near the trailing spot auroral features highlighted in the purple boxes. The magnetospheric observations (Figures 4c – 4i) cover the time range from 03:00 – 05:00 UT. During this timeframe, Juno moved toward Jupiter from 7.8 to 5.8 R_J and to higher northern magnetic latitudes from 42°N to 51°N, and its magnetic footprint mapped near the predicted location of the main emission and the bright UV emissions highlighted in Figures 2. The vertical purple rectangular box highlights particle and field observations that coincide with the timing of the auroral observations in Figures 4a and 4b.

Figure 4(c) shows an energy versus time spectrogram of differential energy flux for 0.1 – 1000 keV electrons based on combined JEDI and JADE-E observations. The JEDI observations (> 100 keV) have a 30 s time resolution throughout this period while the JADE-E observations have a resolution of 1 s from 03:00 –03:30 UT and a 30 s resolution from 03:30 – 05:00 UT. The transition between the JADE and JEDI data presented here is at 100 keV.

The electron distributions show variations in both differential energy flux and energy. The most notable features are the depletions in low-energy electrons observed between ~03:11 – 03:12, 03:18 – 03:26, and 03:53 – 04:25 UT. During these times, the minimum energy of the electrons increases from < ~200 eV to ≥ 10 keV, the bulk of their differential energy flux distributions being at energies > 100 keV, with their maximum energy exceeding 500 keV. A closer inspection of the JEDI data from ~03:18 – 03:26 and 04:00 – 04:15 UT shows an enhanced electron flux just above 160 keV in the electron energy spectrogram. This signature is consistent with the presence of penetrating (> ~1 MeV) electrons. The interval between 03:53 – 04:25 UT contains the period where the electrons map to near the dawn UV emissions highlighted in Figures 4(a) and 4(b), the increase in electron energy being consistent with the high UV color ratio observations.

The pitch angle distributions for the ~30 keV – 1 MeV electrons in Figure 4(d) are primarily between 0 - 30° and 150 - 180°, indicating that the electrons are mostly field-aligned and bi-directional at Juno's location, traveling both towards (downward) and away (upward) from Jupiter. The pitch angles for the 0.1 – 100 keV electrons in Figure 4(e) are also primarily field-aligned and bi-directional, both during times when the low-energy electrons are prominent and when they are depleted. The loss cone at Juno's radial distance during this timeframe ranged from ~2.5° - 4°, which is below the pitch angle resolution for JEDI and JADE.

The 45 – 1000 keV proton and 0.01 – 46 keV/q ion differential energy flux distributions in Figure 4(f) and 4(g), respectively, display similar features as the electrons. Depletions in the low energy ions are observed during similar times as the low energy electrons. At times, the bulk of the ion distributions are at energies above 50 keV. The pitch angle distributions for the protons in Figure 4(f) (not shown) provide evidence for field-aligned, downgoing beams between ~03:20 – 03:30 UT and 04:12 – 04:14 UT.

Figures 4(h) and 4(i) show magnetic field perturbations and magnitudes, respectively, for the radial (B_r), meridional (B_θ), and azimuthal (B_φ) components of Jupiter's magnetic field in a spherical coordinate system. The magnetic field perturbations are calculated by taking the 1 s magnetic field observations and subtracting the ambient field predicted by JRM09 [Connerney et al. 2018] with the latest Jupiter magnetodisc model [Connerney et al. 2020]. During this timeframe, MAG was operating in a range which corresponds to a quantization step size of 0.128nT, indicating that the perturbations recorded here (max ~27 nT) are well resolved. The periods with the largest perturbations occur at ~03:28 – 03:30 UT and ~04:13 – 04:15 UT. Based on the perturbations in B_φ and assuming that all large scale perturbations are associated with a source region, it seems like Juno first crossed a downward field-aligned current region (decreasing δB_φ) followed by an upward field-aligned current region (increasing δB_φ) in both periods mentioned above. The magnetic field magnitude during this interval ranged from ~1500 nT to ~3700 nT. The maximum perturbations recorded here are up to ~0.7% of the ambient field.

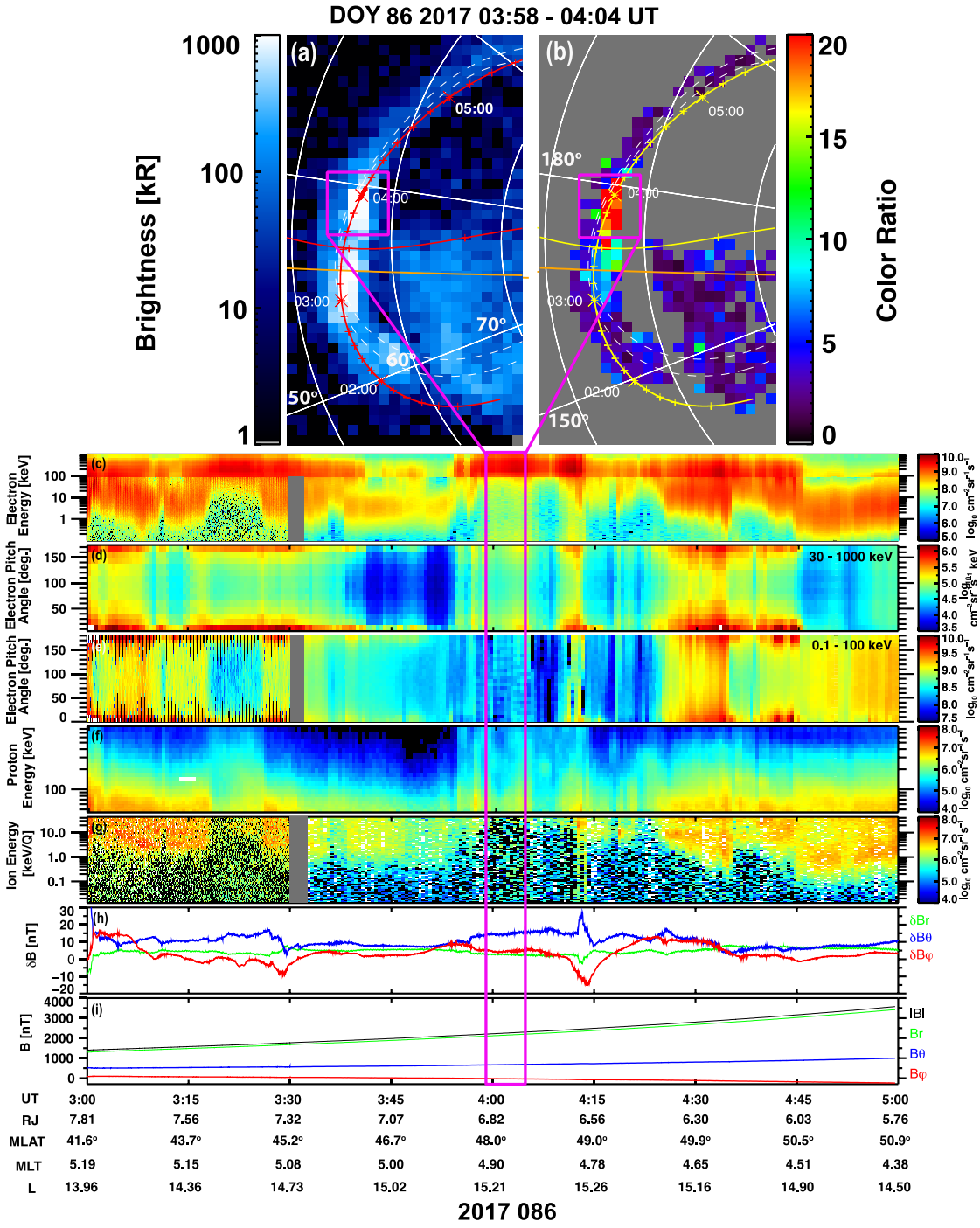

Figure 4: *(a) UV brightness and (b) color ratio images from 03:58 – 04:04 UT on DOY 86, 2017. (c) Energy versus time differential energy flux spectrograms for 0.1– 1000 keV electrons. Electron pitch angle distributions for (d) 30 – 1000 keV and (e) 0.1 – 100 keV electrons, respectively. Electrons with pitch angles of 0° and 180° are moving toward (downward) and away from (upward) Jupiter, respectively. (f) 45 – 1000 keV proton and (g) ~0.01 – 46 keV/q ion differential energy flux spectrograms, respectively. (h) magnetic field perturbations and (i) magnitudes, respectively. The purple boxes identify the UV emission and color ratio features that Juno is mapping to and the corresponding*

magnetospheric observations. Data gaps are denoted by grey pixels. Juno's jovicentric distance (R_J), magnetic latitude (MLAT), magnetic local time (MLT), and M-shell (M), are provided.

Figure 5 displays the plasma wave electric and magnetic spectral density for the time range shown in Figure 4. The electric field frequencies ranged from ~50 – 200,000 Hz and the magnetic field frequencies from 50 – 20000 Hz. The emissions just above the electron cyclotron frequency (f_{ce}) (white line) in the top panel are broadband kilometric radio emissions (bKOM). The bKOM is a free-space mode wave generated by the cyclotron maser instability (CMI) at frequencies above f_{ce}. The bKOM appear to be more intense when electrons having keV energies are present. Multi-instrument studies with JADE and Waves when Juno crossed hectometric (HOM) radio sources show that 5-10 keV electrons are able to produce this radiation via CMI [e.g. Louarn et al., 2017, 2018]. Studies of non-Io-related decametric (non-Io-DAM) emissions estimated the energy of resonant electrons to be in the range of several keV [Imai et al., 2017]. Analogous to HOM and non-Io-DAM radiation, the bKOM resonant energy may also be several keV, which is consistent with the enhanced electron energy observations in Figure 4. More details of these emissions during PJ5 can be found in Imai et al. [2019].

The emission below the f_{ce} are whistler mode auroral hiss with the bulk of the wave energy below 1 kHz. These waves typically propagate along magnetic field lines. Intensification near 03:30 and 04:15 UT correspond to the regions of currents identified in Figure 4(h). When their direction of propagation can be determined (between ~03:23 – 03:25 UT), these whistler mode waves appear to be upward propagating and are likely generated at altitudes below the spacecraft. This technique uses orthogonally oriented B and E sensors (as they are on Juno) to measure the phase between signals in these two sensors. This can provide information on whether the propagation is parallel or anti-parallel to the magnetic field. Details of this technique can be found in Kolmasova et al. [2018].

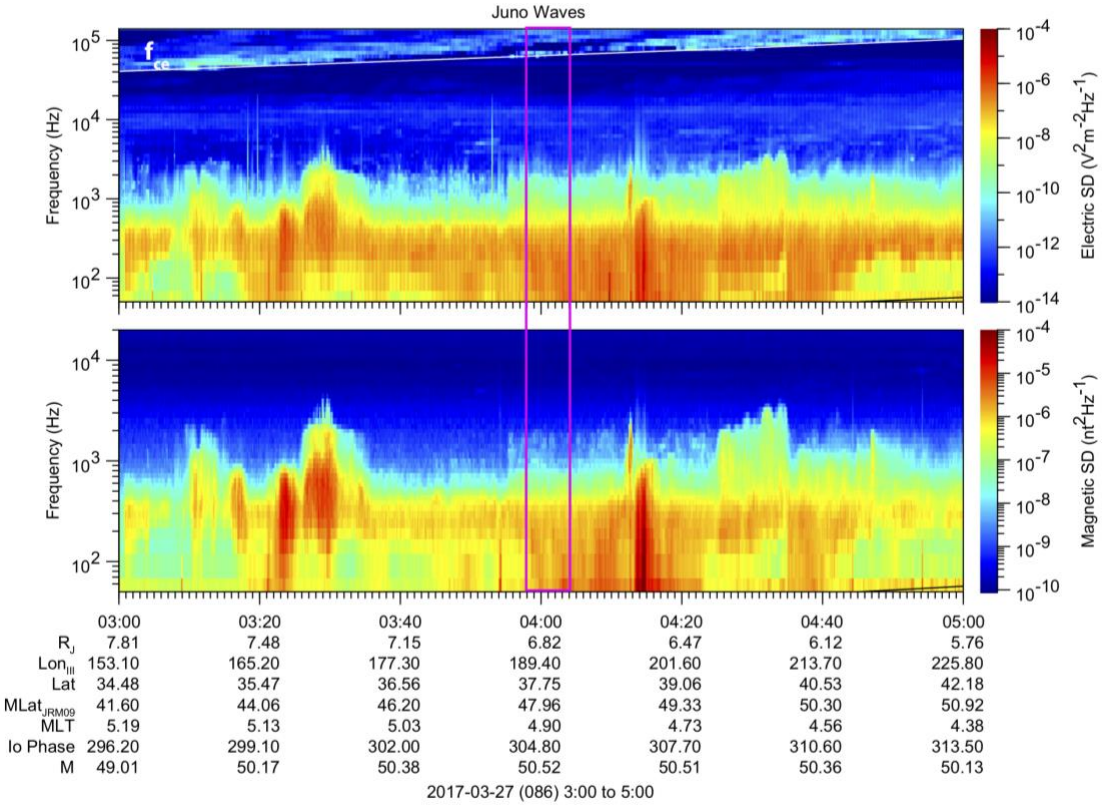

Figure 5: *Time series of plasma wave electric (top) and magnetic (bottom) field spectral density from 03:00 – 05:00 UT on day of year 086, 2017. The white line in the top panel denotes the electron cyclotron frequency (f_{ce}). Juno's jovicentric distance (R_J), system III longitude (LON_{III}), jovigraphic latitude (Lat), magnetic latitude ($MLat_{JRM09}$), magnetic local time (MLT), phase angle relative to Io, and M-shell (M) are provided. The purple box identifies the same interval as highlighted in Figure 4.*

Figure 6 combines JADE-E and JEDI observations to examine the differential intensity versus energy distributions, or energy spectra, of 0.1 – 1000 keV electrons for selected intervals between 03:00 – 05:00 UT on DOY 086, 2017. We highlight periods where the low energy electrons are and are not depleted and when the magnetic field perturbations are largest. The electron energy spectra are separated into field-aligned distributions with pitch angles between 0 – 15º (downward – electrons moving towards Jupiter) and between 165 – 180º (upward – electrons moving towards Jupiter). We only select JADE intervals for times when JADE-E has full pitch angle coverage.

Figure 6a shows the energy spectra during a time when the electron intensities peak at ~ 1 – 2 keV, have a power-law distribution above those energies, and show little difference between the upward and downward intensities. Figures 6(b) – (d) highlight intervals where the low energy electron intensities are depleted and the high energy electrons are enhanced. Note the 1 – 2 order of magnitude increase in the 100 – 1000 keV electron intensities compared to Figure 6(a). Figure 6(c) shows energy spectra within the time interval when Juno was mapping to near the dawn storm UV emissions in Figure 4(a) – (b). Figure 6(d) shows energy spectra during the time when Juno observes the largest magnetic field

perturbations during this interval, noting the possible upward versus downward intensity asymmetry between 1 – 50 keV and 100 – 1000 keV. The upward electrons above 100 keV have higher intensities compared to the downward electrons, indicating that further acceleration may be occurring below Juno's altitude.

The scatter in the JADE intensities in Figures 6(b) – (c) are due to the low energy plasma being tenuous and variable and the measured signal being at or near the one-count level of the instrument. The JADE and JEDI electron spectra show agreement within up to a factor of 2 at overlapping energies. The intensity increases in the JADE-E spectra between ~20 – 100 keV is likely due to residual background signal not being completely removed from the observations [see Allegrini et al. 2020a for details]. Additional factors may include the different temporal resolution for the JADE and JEDI observations presented here and differences in field-of-view and angular resolution between the two instruments as described in Allegrini et al. [2020a]. The distinct bump in intensities observed in all plots between ~150 – 500 keV is due to a JEDI instrument artifact where energetic electrons can begin passing completely through the solid state detectors (SSDs) at ~420 keV, meaning all their energy is not properly captured and instead these particles give false counts around and above about 160 keV. These local peaks can be thought about as the integrated count rate of electrons above 420 keV that escaped detection of their full energy by JEDI [see Mauk et al., 2017c for details]. This feature was partially corrected by redistributing the intensities to their expected energy following the approach outlined in Mauk et al. 2017c.

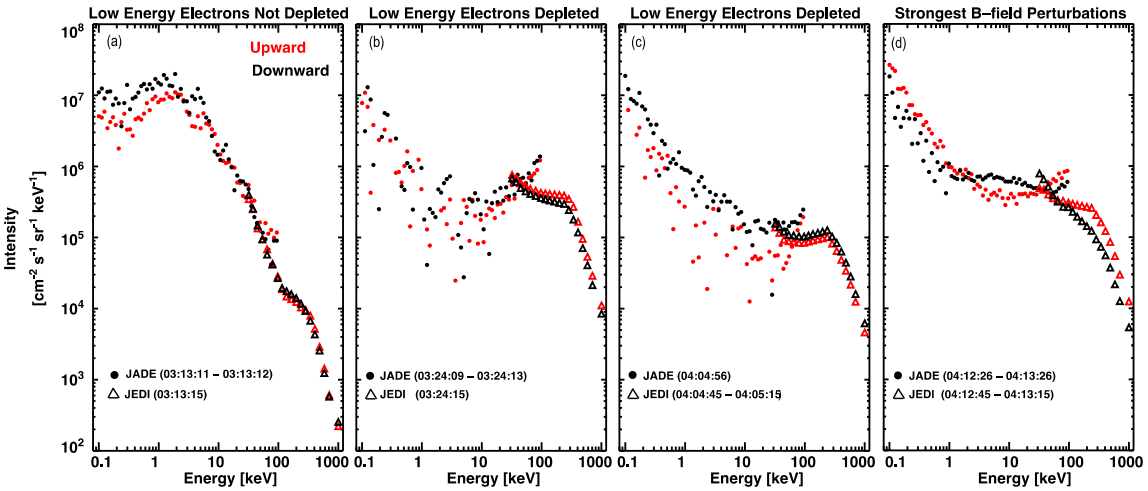

Figure 6: *(a) – (d) Intensity versus energy for 0.1 – 1000 keV electrons in Jupiter's polar magnetosphere. Measurements are from the JADE-E and JEDI instruments on Juno. Black and red symbols represent electron intensities with pitch angles of 0 – 15 °(downward) and 165 –180 °(upward), respectively. The JADE observations in (a) – (b) and (c) – (d) have 1 second and 30 second resolution, respectively, while the JEDI observations have 30 second resolution throughout. The intensities from each instrument are averaged over the time interval specified in each plot.*

Table 1 provides estimates for the characteristic energy and energy flux of the electron distributions in Figure 6. Both quantities are calculated using methods described in several recent Juno studies [e.g. Mauk et al. 2017b, Clark et al. 2018, Allegrini et al. 2020a]. The

characteristic energy reflects the average energy of the electron distributions while the energy flux is a measure of the electron power per unit area. We use JADE observations from 0.1 – 50 keV and JEDI observations from 50 – 1000 keV in the calculation. The characteristic energy for the upward and downward electron distributions in Figure 6(a) were 24 and 19 keV, respectively, while their energy flux was 9 – 10 mW m^{-2}. The characteristic energy and energy flux associated with the distributions in Figures 6(b) – (d), where the low energy electrons are depleted and high energy electron intensities are enhanced, were a factor of 5 – 20 larger. In particular, the downward energy fluxes in these intervals contain significant fraction of the values required to produce the dawn storm UV emissions identified in Figures 2 – 4, assuming a factor of 10 conversion between energy flux and UV brightness (1 mW m^{-2} ~ 10 kR) [e.g. Grodent et al., 2001], though we note that neither JADE or JEDI are able to resolve the loss cone at the altitude of these observations.

Table 1: Characteristic Energy and Energy Flux for the Electron Distributions in Figure 6.

Time Interval on DOY 86, 2017 (UT)	Characteristic Energy [keV]		Energy Flux [mW m^{-2}]	
	Upward	Downward	Upward	Downward
JADE: 03:11:11 – 03:11:12 JEDI: 03:11:15	24	19	9	10
JADE: 03:24:09 – 03:24:13 JEDI: 03:24:15	235	212	179	134
JADE: 04:04:56 JEDI: 04:04:45 – 04:05:15	283	247	51	66
JADE: 04:12:26 – 04:13:26 JEDI: 04:12:45 – 04:13:15	221	163	137	69

4. Discussion

We present in situ and remote sensing observations from Juno that connect electrons, ions, magnetic field, and plasma waves in Jupiter's northern polar magnetosphere to transient UV emissions near Jupiter's northern main aurora. The transient UV emissions, consisting of two separate, elongated structures with high color ratios, were observed in the dawn region near the main aurora, extended into the nightside, and rotated to the dayside, suggesting that the generation process of these UV emissions was located in the middle magnetosphere [e.g. Clarke et al., 1998], and moving in the direction of Jupiter's rotation.

These UV emissions have similar characteristics as the UV brightenings described by Gustin et al., [2006] (high color ratios, leading edge traveling in the direction of planetary rotation, trailing edge extending into the nightside), features that are often attributed to dawn storms. According to Bonfond et al. [2021], dawn storms originate near midnight and are initially fixed in magnetic local time. The UV emissions then brighten, their color ratios increasing, as they move towards dawn and are observed to corotate with the planet. Kimura et al., [2017] noted that after onset, dawn storms expand in latitude and longitude, have a rapid increase in total UV power, and produce emissions equatorward of the main auroral oval, during the peak phase of the storm. The UV emissions presented here are consistent with several of these dawn storm features. It was indeed identified as such in

Bonfond et al. [2021] and was followed by another dawn storm starting at 07:33 UT on the same day. These dawn storm emissions had a peak UV brightness of at least 1.4 MR and the emissions dimmed as they rotated to Jupiter's dayside. The color ratios show a similar trend, peaking between ~30 and ~70 for the leading and trailing emissions, respectively, and reducing significantly as the UV emissions rotated towards the dayside. This suggests that both the energy flux and energy of the electrons producing these emissions were also decreasing. Both the UV brightness and color ratio remained enhanced compared to the surrounding UV emissions for the period examined here.

The electron distributions presented here show several distinct characteristics. At times, the bulk of the electron intensities reside between ~1 – 100 keV, extend to as low as ~100 – 200 eV and are field-aligned. We interpret these observations as plasma sheet electrons with high latitude mirror points. During other times, the electron intensities are depleted at energies below < 10 keV, are enhanced at energies of 100s keV, and are also field-aligned. The signature of energetic populations measured simultaneously with depleted lower energies is often associated with the interchange process, whereby flux tube bundles of energized particles (perhaps moving inward and gaining energy by the conservation of the first adiabatic invariant, μ) displace colder plasma in the region. The ions have similar energy distributions as the electrons and at concurrent times. These cold and hot electron and ion populations are interspersed and likely reflect a large-scale dynamic process in Jupiter's equatorial magnetosphere at this time, where ambient plasma in Jupiter's middle magnetosphere is accelerated, heated, and transported to high latitude. For example, Swithenbank-Harris et al. [2021] reported enhanced hot plasma densities at ~ 60 R_J, including field-aligned protons and heavy ions, along with reversals of the azimuthal magnetic field, in the equatorial dawn magnetosphere during the dawn storm observed by HST on July 13, 2016. They attribute the heating and acceleration of the equatorial plasma to processes associated with magnetic reconnection and/or disruption of the azimuthal current. Similar processes may be responsible for accelerating the electrons and ions for the dawn storm reported here, prior to them being transported to high latitude.

The characteristic energy and energy flux of the hot electrons reported here are between a factor of 5 – 20 larger than the cold distributions. The characteristic hot downward electron energies of ~160 – 250 keV provide further evidence that dawn storms are produced by energetic, 100s of keV, electrons. This is consistent with the high color ratio observations for this event and the long-standing interpretation based on electron energy estimates derived from color ratios of remotely sensed UV emissions from Jupiter's auroral region [e.g., Gustin et al., 2006]. The hot electron distributions contain a significant fraction of the energy flux required to produce the UV brightness of at least ~0.5 – 1.4 MR for this dawn storm, even at Juno's radial distance of 6 – 8 R_J, with further enhancements possible closer to the planet. Since neither JADE nor JEDI can resolve the loss cone at the radial distance of these observations, however, we cannot make a definitive statement about the electron distributions that are precipitating into the atmosphere to produce these dawn storm emissions.

The upward to downward asymmetry in intensity, characteristic energy, and energy flux observed in some of the electron energy spectra presented above indicate that further

acceleration is occurring below Juno's altitude during these events. The wave observations during this period suggest that whistler mode auroral hiss and broadband kilometric (bKOM) radio emissions are present at and/or below Juno's altitude. Previous studies have shown whistler mode waves to be associated with electron beams and which could further energize and pitch-angle scatter the electrons [e.g., Elliott et al. 2018; Sulaiman et al., 2020]. According to Imai et al. [2019], the intensity of bKOM radio emissions for this northern pass is positively correlated with the UV brightness and color ratio within radio source footprints. These positive correlations imply the existence of particles to wave energy transport (i.e. some of the weakly relativistic electron energy converts into the bKOM wave energy) along the common magnetic field lines between the bKOM radio sources and the UV emissions.

The significant magnetic field perturbations observed at ~03:28 – 03:30 UT, and especially at ~04:13 – 04:15 UT, coupled with the field-aligned and bi-directional nature of the electron pitch angle distributions, provide evidence that field aligned currents are also connected with these events. These perturbations are up to 0.7% of the ambient field at Juno's location, a similar percentage as the magnetic perturbations measured closer to the planet driven by field-aligned currents associated with Jupiter's main aurora [Kotsiaros et al., 2019].

One candidate for producing these auroral emissions is plasma injections [e.g., Mauk et al., 1997], where hot, tenuous plasma is radially transported planetward while cold, dense plasma is transported outward [e.g., Dumont et al., 2014]. Plasma injections are thought to be produced by processes related to interchange instability [Thorne et al., 1997; Mauk et al., 1999] and/or tail reconnection [e.g., Krupp et al., 1998; Louarn et al., 2014; Gray et al., 2016; Kimura et al., 2017]. Mauk et al., [2002] proposed two mechanisms for how plasma injections can produce auroral emissions at Jupiter. The first is electron scattering by magnetospheric waves that modify the electron pitch angle distribution by scattering electrons into the loss cone. Simulations by Dumont et al., [2018] suggested that electron pitch angle scattering by whistler mode waves could reproduce the auroral signatures associated with plasma injections. The second mechanism involves a current driven along the pressure gradient between the injected plasma and the surrounding plasma, which must close at the planet. These currents interact with plasma near the planet to produce downward accelerated electrons and auroral emissions that map to the trailing edge of the injected hot plasma distribution that's rotating with Jupiter. The electron distributions associated with the dawn storm emissions studied here were energetic (100s of keV), field-aligned, and bi-directional at Juno's location (6 – 8 R_J jovicentric distance, 40 – 50°N magnetic latitude), providing evidence that currents were flowing both towards and away from Jupiter or electrons were accelerated toward Jupiter and mirrored back. These observations are more consistent with the second mechanism being the driver of these emissions, even though these are not necessarily mutually exclusive. The presence of whistler mode auroral hiss at and below Juno's altitude may provide a mechanism for electrons being further energized and scattered into the loss cone as they travel from Juno's location to Jupiter atmosphere.

More recently, Yao et al. [2020] analyzed HST observations of Jupiter's auroral region and found several instances where auroral emissions associated with dawn storms and with injection events were observed at the same time. Examination of in-situ measurements from Juno during one of these intervals revealed evidence of magnetic reconnection in the pre-dawn sector of the equatorial magnetosphere, followed by signatures of magnetic dipolarization a few hours later. The interpretation of these combined observations was that magnetic reconnection and the resulting reconfiguration of the field lines inward of the X-line in the dawn magnetosphere was responsible for the dawn storms and the regions of magnetic dipolarization that co-rotated with the planet were associated with plasma injections that eventually produced the auroral injection emissions. They suggested a physical connection for these two types of transient auroral emissions with magnetic perturbations being a common feature of both processes. We note that magnetic perturbations were also observed at high latitude during times when Juno was mapping to near the dawn storm studied here, providing further evidence that field line reconfiguration may be associated with these events.

The processes that accelerate the plasma associated with these dawn storms, both in the equatorial magnetosphere and at high latitude near the planet, are not fully understood. The observed electron distributions mapping to the dawn storm emissions that carry the largest energy fluxes are broad in energy, ranging from 1 – 10s of keV up to 1000 keV, with significant intensity depletions below ~1 keV. Broad energy distributions are often attributed to stochastic particle acceleration (as opposed to acceleration by electrostatic potentials which show a mono-energetic peak in the intensity-energy distributions). Stochastic acceleration appears to be significant in energizing electrons that produce UV emissions associated with Jupiter's diffuse [Li et al. 2017], main [Mauk et al. 2017a, 2020, Allegrini et al. 2017, 2020a], polar [Ebert et al. 2017, 2019], and satellite footprint [Allegrini et al. 2020b, Szalay et al. 2018, 2020] aurora. Proposed mechanisms include dissipation of turbulent Alfvénic fluctuations [Saur et al. 2003], resonance with whistler mode waves [Kurth et al. 2018, Elliott et al. 2018], electron Landau damping of kinetic Alfvén waves [Saur et al. 2018], incompressible magnetic (Alfvénic) turbulence [Gershman et al. 2019; Sulaiman et al., 2020] and magnetospheric ultra-low frequency (1 – 60 min) Alfvénic waves [Pan et al. 2021]. It is recommended that follow-up work focus on whether stochastic or other processes are responsible for accelerating the electrons that produce these dawn storm emissions.

5. Summary and Conclusions

We presented a multi-instrument analysis of a UV dawn storm observed in Jupiter's northern auroral region prior to Juno perijove 5, sampling magnetic field lines at high-latitude while remotely observing UV auroral emissions. We combined in situ plasma, energetic particle, magnetic field, and wave observations between 6 – 8 R_J in jovicentric distance and 40 – 50°N in magnetic latitude with images of UV brightness and color ratio. The dawn storm UV emissions had brightness up to at least 1.4 MR and high color ratios that indicated a deeper atmospheric penetration depth for the auroral-producing electrons compared to those producing the surrounding UV emissions. Both the brightness and color ratio of these emissions decreased with time as they rotated towards the dayside, indicating

that the energy flux and energy of the electrons producing them was also decreasing. The electron distributions were field-aligned, bi-directional and variable in energy, providing evidence for field aligned-currents. The electrons mostly likely producing the dawn storm emissions had broad energy distributions between ~10 – 1000 keV, significant intensity depletions below 10 keV, characteristic energies from ~160 – 250 keV and downward energy fluxes from ~70 – 130 mW m^{-2} at Juno's altitude. The ion distributions had similar energy distributions at similar times as the electrons, suggesting that they are being accelerated by similar processes. Magnetic perturbations as large as 27 nT, or ~0.7% of the local magnetic field, were observed on field lines that mapped to the dawn storm with variations in B_φ and B_θ providing evidence of upward and downward currents. Whistler mode waves and broadband kilometric radio emissions were also observed.

Based on these observations, we conclude the following:

1. These dawn storm emissions were generated by processes that mapped to Jupiter's nightside and then traveled in the direction of planetary rotation.

2. The high latitude energetic electron and ion populations measured simultaneously with depleted lower energies are similar to particle observations in the equatorial magnetosphere associated with dynamic processes driven by interchange events, plasma injections, and/or tail reconnection.

3. The electron distributions associated with these dawn storm emissions were field-aligned and had characteristic energies in the 100s of keV range and energies up to at least 1 MeV.

4. The particles were energized prior to arriving at Juno's location, the electron distributions already containing a significant fraction of the energy flux needed to produce the dawn storm UV emissions.

5. The magnetic field perturbations suggestive of upward and downward currents, combined with the field-aligned, bi-directional electrons, indicate that field-aligned currents are associated the processes driving these dawn storm emissions.

6. Whistler mode waves may play a role in enhancing these dawn storm UV emissions while the enhanced broadband kilometric radiation may be a result of one-way energy transport from these dawn storm particles into waves.

Acknowledgements

This work was supported as a part of the work on the Jovian Auroral Distributions Experiment (JADE) and Juno Ultraviolet Spectrograph (Juno UVS) on NASA's Juno mission. The Jovian Energetic particle Detector Instrument (JEDI) work was funded by NASA's New Frontiers Program for Juno via a subcontract with the Southwest Research Institute. The research at the University of Iowa was supported by NASA through Contract

699041X with the Southwest Research Institute. This work was supported at the University of Colorado as a part NASA's Juno mission supported by NASA through contract 699050X with the Southwest Research Institute. The work of MI was supported by the JSPS KAKENHI Grant Number JP20K22371.

The Juno data is available at NASA's Planetary Data System (https://pds.nasa.gov) and the following DOIs. The JADE data used for this study is from dataset ID JNO-J/SW-JAD-3-CALIBRATED-V1.0 (doi: 10.17189/1519715), in particular the Version 02 and 03 files from the ion time-of-flight and electron data, respectively. The JEDI data are from dataset ID JNO-J-JED-3_CDR-V1.0. The MAG data are from dataset ID JNO-J-3-FGM-CAL-V1.0 found at https://doi.org/10.17189/1519711. The Juno Waves data are at https://doi.org/10.17189/1519710. The UVS data are from dataset ID JNO-J-UVS-3-RDR-V1.0 which can be found at https://doi.org/10.17189/1518951.

References

Allegrini, F., et al. (2017), Electron beams and loss cones in the auroral regions of Jupiter, *Geophys. Res. Lett.*, 44, 7131–7139, doi:10.1002/2017GL073180.

Allegrini, F. et al. (2020a), Energy flux and characteristic energy of electrons over Jupiter's main auroral emission, *J. Geophys. Res.*, 125, e2019JA027693. https://doi.org/10.1029/2019JA027693

Allegrini, F., Gladstone, G. R., Hue, V., Clark, G., Szalay, J. R., Kurth, W. S., et al. (2020b). First report of electron measurements during a Europa footprint tail crossing by Juno, *Geophys. Res. Lett.*, 47, e2020GL089732, https://doi.org/10.1029/2020GL089732.

Ballester, G. E. et al. (1996), Time-resolved observations of Jupiter's far-ultraviolet aurora, *Science*, 274, 5286, 409 – 413.

Bolton, S. J., Lunine, J. Stevenson, D., Connerney, J. E. P., Levin, S., et al. (2017), The Juno mission, *Space Sci Rev.*, 213, 1 – 4, p. 5-37.

Bonfond, B., et al. (2012), Auroral evidence of Io's control over the magnetosphere of Jupiter, *Geophys. Res. Lett.*, 39, L01105, doi:10.1029/2011GL050253.

Bonfond, B. et al. (2021), Are Dawn Storms Jupiter's Auroral Substorms? *AGU Advances*, 2, e2020AV000275. https:/doi.org/10.1029/2020AV000275.

Broadfoot, A. L. et al. (1979), Extreme Ultraviolet Observations from Voyager 1 Encounter with Jupiter, *Science*, 204, 4396, 979 – 982.

Clark, G. et al. (2018), Precipitating electron energy flux and characteristic energies in Jupiter's main auroral region as measured by Juno/JEDI, *J. Geophys. Res.*, 123 (9), 7554 – 7567.

687 Clarke, J. T. et al. (1998), Hubble Space Telescope imaging of Jupiter's UV aurora
688 during the Galileo orbiter mission, *J. Geophys. Res.*, 103, E9, 20217 – 20236.
689
690 Connerney, J. E. P., M. H. Acuna, and N. F. Ness (1981), Modeling the Jovian current
691 sheet and inner magnetosphere, *J. Geophys. Res.*, 86, 8370–8384.
692
693 Connerney, J. E. P., et al. (2017a). Jupiter's magnetosphere and aurorae observed by the
694 Juno spacecraft during its first polar orbits, *Science*, *356*(6340), 826 –
695 832. https://doi.org/10.1126/science.aam5928
696
697 Connerney, J. E. P., et al. (2017b) The Juno Magnetic Field Investigation, *Space Sci. Rev.*,
698 213, 1 – 4, doi: 10.1007/s11214-017-0334-z.
699
700 Connerney, J. E. P., Kotsiaros, S., Oliversen, R. J., Espley, J. R., Joergensen, J. L., et al.
701 (2018), A new model of Jupiter's magnetic field from Juno's first nine orbits, *Geophys.*
702 *Res. Lett.*, 45, 6, 2590 – 2596.
703
704 Connerney, J. E. P., et al. (2020), A Jovian magnetodisc model for the Juno Era, *J. Geophys.*
705 *Res.*, 125(10), e2020JA028138.
706
707 Dumont, M., D. Grodent, A. Radioti, B. Bonfond, and J.-C. Gérard (2014), Jupiter's
708 equatorward auroral features: Possible signatures of magnetospheric injections, *J. Geophys.*
709 *Res.*, 119, 10,068 – 10,077, doi: 10.1029/2018JA025708.
710
711 Dumont, M. et al., (2018), Evolution of the auroral signatures of Jupiter's magnetosphere
712 injections, *J. Geophys. Res.*, 123, 8489 – 8501.
713
714 Ebert, R. W., et al. (2017), Spatial distribution and properties of 0.1 – 100 keV electrons in
715 Jupiter's polar aurora region, *Geophys. Res. Lett.*, *44*, 18, 9199 – 9207,
716 doi://10.1002/2017GL075106.
717
718 Ebert, R. W. et al. (2019), Comparing electron energetics and UV brightness in Jupiter's
719 northern polar auroral region prior for Juno perijove 5, *Geophys. Res. Lett.*, 46(1), 19 – 27,
720 doi: 10.1029/2018GL081129.
721
722 Elliott, S. S. et al. (2018), The acceleration of electrons to high energies over the Jovian
723 polar cap via whistler mode wave-particle interactions, *J. Geophys. Res.*, 123 (9), 7523 –
724 7533.
725
726 Gérard, J.-Cl. and V. Singh (1982), A model of energy deposition of energetic electrons
727 and EUV emission in the Jovian and Saturnian atmospheres and implications, *J.*
728 *Geophys. Res.*, 87, A6, 4524 – 4532.
729
730 Gérard, J.-C. et al. (1994), A remarkable auroral event on Jupiter observed in the ultraviolet
731 with the Hubble Space Telescope, *Science*, 266, 1675 – 1678.
732

Gérard, J.-C., B. Bonfond, D. Grodent, A. Radiotti, J. T. Clarke et al. (2014), Mapping the electron energy in Jupiter's aurora: Hubble spectral observations, *J. Geophys. Res. Space Physics*, 119, doi:10.1002/2014JA020514.

Gérard, J.-C., B. Bonfond, B. Mauk, G.R. Gladstone, Z.H. Yao, T.K. Greathouse, et al. (2019). Contemporaneous observations of Jovian energetic auroral electrons and ultraviolet emissions by the Juno spacecraft, *J. Geophys. Res.: Space Physics*, 124, 8298–8317. https://doi.org/10.1029/2019JA026862.

Gershman, D. J., Connerney, J. E. P., Kotsiaros, S., DiBraccio, G. A., Martos, Y. M., F.-Viñas, A., et al (2019). Alfvénic fluctuations associated with Jupiter's auroral emissions. *Geophys. Res. Lett.*, 46, 13, 7157-7165. https://doi.org/10.1029/2019GL082951.

Gladstone, G. R., et al. (2017), The ultraviolet spectrograph on NASA's Juno mission, *Space Sci. Rev.*, 213, 1 – 4, doi:10.1007/s11214-014-0040-z.

Gray, R. L., Badman, S. V., Bonfond, B., Kimura, T., Misawa, H., Nichols, J. D., et al. (2016). Auroral evidence of radial transport at Jupiter during January 2014. *J. Geophys. Res.: Space Physics*, 121, 9972–9984. https://doi.org/10.1002/2016JA023007

Grodent, D., J. H. Waite Jr., and J.-C. Gérard (2001), A self-consistent model of the Jovian auroral thermal structure, *J. Geophys. Res.*, 106, 12,933 – 12,952.

Grodent, D., et al. (2003), Jupiter's polar aurora emissions, *J. Geophys. Res.*, 108, A10, SMP 6-1, CiteID 1366, doi:10.1029/2003JA010017.

Grodent, D., (2015), A brief review of ultraviolet auroral emissions on giant planets, *Space Sci. Rev.*, 187, 23 – 50.

Gustin, J., S. W. H. Cowley, J.-C. Gérard, G. R. Gladstone, D. Grodent, and J. T. Clarke (2006), Characteristics of jovian morning bright FUV aurora form Hubble Space Telescope/space telescope imaging spectrograph imaging and spectral observations, *J. Geophys. Res.*, 111, A09220.

Imai, M., W. S. Kurth, G. B. Hospodarsky, S. J. Bolton, J. E. P. Connerney, S. M. Levin, A. Lecacheux, L. Lamy, and P. Zarka (2017), Latitudinal beaming of Jovian decametric radio emissions as viewed from Juno and the Nançay Decameter Array, *Geophys. Res. Lett.*, 44, 4455–4462, doi:10.1002/2016GL072454.

Imai, M. et al. (2019), Probing Jovian kilometric radio sources tied to the ultraviolet main auroral oval with Juno, *Geophys. Res. Lett.*, 46(2), 571 – 579.

Kimura, T. et al. (2015), Transient internally driven aurora at Jupiter discovered by Hisaki and the Hubble Space Telescope, *Geophys. Res. Lett.*, 42, 1662 – 1668.

779 Kimura et al. (2017), Transient brightening of Jupiter's aurora observed by the Hisaki
780 satellite and Hubble Space Telescope during approach phase of the Juno spacecraft,
781 *Geophys. Res. Lett.*, 44, 4523 – 4531.
782
783 Kolmasova, I., M. Imai, O. Santolik, W. S. Kurth, G. B. Hospodarsky, D. A. Gurnett,
784 J.E.P. Connerney, and S. J. Bolton (2018), Discovery of rapid whistlers close to Jupiter
785 implying similar lightning rates as on Earth, *Nature Astronomy*, 2(7), 544-
786 548. https://doi.org/10.1038/s41550-018-0442-z.
787
788 Kotsiaros, S., Connerney, J.E.P., Clark, G., Allegrini, F., Gladstone, G.R., Kurth, et al.
789 (2019). Birkeland currents in Jupiter's magnetosphere observed by the polar-orbiting Juno
790 spacecraft, *Nature Astronomy*, 3, 904-909. DOI: 10.1038/s41550-019-0819-7
791
792 Krupp, N., J. Woch, A. Lagg, B. Wilken, S. Livi, and D. J. Williams (1998), Energetic
793 particle bursts in the predawn jovian magnetotail, *Geophys. Res. Lett.*, 25(8), 1249 –
794 1252.
795
796 Kurth, W. S., G. B. Hospodarsky, D. L. Kirchner, B. T. Mokrzycki, T. E. Averkamp et al.
797 (2017), The Juno Waves Investigation, *Space Sci. Rev.*, 213, 347-392,
798 doi:10.1007/s11214-017-0396-y.
799
800 Kurth, W. S., Mauk, B. H., Elliott, S. S., Gurnett, D. A., Hospodarsky, G. B., Santolik,
801 O., et al. (2018). Whistler mode waves associated with broadband auroral electron
802 precipitation at Jupiter, *Geophys. Res. Lett.*, 45(18), 9372-9379.
803 https://doi.org/10.1029/2018GL078566.
804
805 Li, W. et al. (2017), Understanding the origin of Jupiter's diffuse aurora using Juno's first
806 perijove observations, *Geophys. Res. Lett.*, 44, 10,162–10,170.
807 https://doi.org/10.1002/2017GL075545.
808
809 Louarn, P., Andre, N., Jackman, C., Kasahara, S., Kronberg, E., & Vogt, M. (2014).
810 Magnetic reconnection and associated transient phenomena within the magnetospheres of
811 Jupiter and Saturn. *Space Sci. Rev.*, 187, 181–227. https://doi.org/10.1007/s11214-014-
812 0047-5
813
814 Louarn, P., et al. (2017), Generation of the Jovian hectometric radiation: First lessons
815 from Juno, Geophys. Res. Lett., 44, 4439–4446, doi:10.1002/ 2017GL072923.
816
817 Louarn, P., Allegrini, F., McComas, D. J., Valek, P. W., Kurth, W. S., André, N., et al.
818 (2018). Observation of electron conics by Juno: Implications for radio generation and
819 acceleration processes. *Geophys. Res. Lett.*, 45, 9408–9416.
820 https://doi.org/10.1029/2018GL078973
822
823 Mauk, B. H., D. J. Williams, and R. W. McEntire (1997), Energy-time dispersed charged
824 particle signatures of dynamic injections in Jupiter's inner magnetosphere, *Geophys. Res.*
825 *Lett.*, 24(23), 2949 – 2952.

826
827 Mauk, B. H., D. J. Williams, R. W. McEntire, K. K. Khurana, and J. G. Roederer (1999),
828 Storm-like dynamics of Jupiter's inner and middle magnetosphere, *J. Geophys. Res.*, 104
829 (A10), 22,759 – 22,778.
830
831 Mauk, B. H, J. T. Clarke, D. Grodent, J. H. Jr. Waite, C. P. Paranicas, and D. J. Williams
832 (2002), Transient aurora on Jupiter from injection of magnetospheric electrons, *Nature*,
833 415, 1003 – 1005.
834
835 Mauk, B. H., et al. (2017a), The Jupiter energetic particle detector instrument (JEDI)
836 investigation for the Juno mission, *Space Sci. Rev.*, 213(1-4), 289–346.
837 doi:10.1007/s11214-013-0025-3.
838
839 Mauk, B. H. et al. (2017b), Juno observations of energetic charged particles over
840 Jupiter's polar regions: Analysis of mono- and bi-directional electron beams, *Geophys.*
841 *Res. Lett.*, 44, 4410-4418, doi:10.1002/2016GL072286.
842
843 Mauk, B. H., Haggerty, D. K., Paranicas, C., Clark, G., Kollmann, P., Rymer, A. M., et
844 al. (2017c). Discrete and broadband electron acceleration generating Jupiter's uniquely
845 powerful aurora. *Nature*, 549(7670), 66–69. https://doi.org/10.1038/nature23648
846
847 Mauk, B. H. et al. (2020), Energetic particles and acceleration regions over Jupiter's polar
848 cap and main aurora; a broad overview, *J. Geophys. Res.*, 125, 3, e2019JA027699
849 https://doi.org/10.1029/2019JA027699
850
851 McComas, D. J., et al. (2017), The Jovian auroral distributions experiment (JADE) on the
852 Juno mission to Jupiter, *Space Sci. Rev.*, 213, 1 – 4, doi: 10.1007/s11214-013-9990-9.
853
854 Pan, D-X., Yao, Z-H., Manners, H., Dunn, W., Bonfond, B., Grodent, D., et al.
855 (2021). Ultralow-frequency waves in driving Jovian aurorae revealed by observations
856 from HST and Juno. *Geophys. Res. Lett.*, 48,
857 e2020GL091579, https://doi.org/10.1029/2020GL091579
858
859 Prangé, R. et al. (1993), Correlated variations of UV and radio emissions during an
860 outstanding jovian auroral event, *J. Geophys. Res.*, 98, 18,779 – 18,791.
861
862 Radioti, A. D., D. Grodent, J. C. Gérard, B. Bonfond, and J. T. Clarke (2008), Auroral
863 polar dawn spots: Signatures of internally driven reconnection processes at Jupiter's
864 magnetotail, *Geophys. Res. Lett.*, 35, L03104.
865
866 Saur, J., A. Pouquet, and W. H. Matthaeus (2003), An acceleration mechanism for the
867 generation of the main auroral oval on Jupiter, *Geophys. Res. Lett.*, 30, 1260, 319
868 doi:10.1029/2002GL015761.
869
870 Saur, J., Janser, S., Schreiner, A., Clark, G., Mauk, B. H., Kollmann P., et al. (2018). Wave-
871 particle interaction of Alfvén waves in Jupiter's magnetosphere: Auroral and

872 magnetospheric particle acceleration. *Journal of Geophysical Research: Space Physics*,
873 123, 9560–9573. https://doi.org/10.1029/2018JA025948
874
875 Sulaiman, A. H., Hospodarsky, G. B., Elliott, S. S., Kurth, W. S., Gurnett, D. A., Imai, M.,
876 et al. (2020). Wave-Particle Interactions Associated With Io's Auroral Footprint: Evidence
877 of Alfvén, Ion Cyclotron, and Whistler Modes, *Geophys. Res. Lett.*, 47(22),
878 e2020GL088432. https://doi.org/https://doi.org/10.1029/2020GL088432.
879
880 Swithenbank-Harris, B. G. et al. (2021), Simultaneous Observation of an Auroral Dawn
881 Storm with the Hubble Space Telescope and Juno, *Journal of Geophysical Research: Space*
882 *Physics*, 126, e2020JA028717. https://doi.org/10.1029/2020JA028717.
883
884 Szalay, J. R., Bonfond, B., Allegrini, F., Bagenal, F., Bolton, S., Clark, G., et al. (2018). In
885 situ observations connected to the Io footprint tail aurora, *Journal of Geophysical Research:*
886 *Planets*, 123. https://doi.org/10.1029/2018JE005752
887
888 Szalay, J. R. et al. (2020), Alfvénic acceleration sustains Ganymede's footprint tail
889 aurora, *Geophys. Res. Lett.*, 47, e2019GL086527.
890 https://doi.org/10.1029/2019GL086527.
891
892 Thorne, R. M. et al. (1997), Galileo evidence for rapid interchange transport in the Io torus,
893 *Geophys. Res. Lett..*, 24(17), 2131 – 2134.
894
895 Yao, Z. H., Bonfond, B., Clark, G.,Grodent, D., Dunn, W. R., Vogt, M. F., et al. (2020).
896 Reconnection‐and dipolarization‐driven auroral dawn storms and injections. Journal
897 of Geophysical Research: Space Physics, 125, e2019JA027663.
898 https://doi.org/10.1029/2019JA027663